Scaling of convective boundary layer flow induced by linear thermal forcing at Pr < 1 and Pr > 1

Yang Liu*

School of Ocean Science and Technology, Dalian University of Technology, Dalian, 116024, China

(Received 14 July 2019; published 21 October 2019)

The transient convective boundary layer flow induced by heating an initially isothermal and stationary fluid with a linearly heated semi-infinite vertical plate is comprehensively investigated by a scaling analysis in the present study. The local temperature at the leading edge of the specified linear thermal profile can be any value that is no lower than the ambient fluid, which significantly differentiates the present study from previous similar investigations. Additionally, the convective flow associated with both Pr $<$ 1 and Pr $>$ 1 (where Pr is the Prandtl number) fluids is analyzed and quantified. The derived scaling relations demonstrate that the dynamics of the Pr $<$ 1 and Pr $>$ 1 fluids are fundamentally different and the two flows are described by different sets of scaling laws. The study also shows that the convective boundary layer flow first experiences an initial growth state, and it eventually transits to a fully steady state after the leading edge effect has been completely convected away. It is further revealed that unlike the extensively studied homogenously heating problem which is featured by a one-dimensional initial growth state and a two-dimensional fully developed state, the present flow is consistently two-dimensional if a nonzero background temperature stratification presents. The derived scaling relations are validated against the direct numerical simulation results, and a good agreement is obtained.

DOI: 10.1103/PhysRevE.100.043112

I. INTRODUCTION

Convective flow adjacent to a heated vertical surface is a crucial problem in many industrial processes, such as cooling of microchips, solar chimneys, operation of nuclear reactors, and autonomous ventilation of next-generation high-rise buildings. This problem has been investigated for more than a century since the ground-breaking boundary layer theory was first proposed by Prandtl in 1904 [1,2]. Over the years, various aspects of the boundary layer flow have been intensively studied [3–12], and the corresponding research outcomes have directly or laterally facilitated the design of electronic cooling devices, room radiators, solar collectors, etc. Among the various topics investigated, the instability characteristics, similarity solution, and scaling laws of the convective boundary layer flow are probably the three most important and fundamental ones.

It was suggested that the convective boundary layer experiences three major flow states as the governing Rayleigh number increases: a stable state, a convective unstable state, and an absolute unstable state [13,14]. These three states correspond to different flow regimes and features. The linear stability theory has been proven to be a powerful tool to identify the critical Rayleigh numbers for the regime transitions. In recent decades, this method has been extensively utilized to study the stability and obtain the neutral curve of various convective flow problems.

A linear stability analysis of a buoyant layer was carried out by Tao [14]. The considered convective flow was induced by heating a thermally stratified medium by a vertical hot plate. It was revealed that the disturbed boundary layer flow does not necessarily converge to the basic state, and it can also oscillate with an intrinsic frequency which can be determined by a modified Grashof number. The numerically obtained front position of globally unstable waves agrees very well with that of marginal absolute instability. The dominant frequencies in the oscillating region are also identical to the marginal absolute frequency derived from the local linear dispersion relation. It was therefore concluded that the front of the nonlinear global modes is of a pulled type for the buoyancy-driven flow system considered.

The transition to chaos of the flow between two differentially heated vertical plates was studied by Gao *et al.* [15]. It was demonstrated that after the first bifurcation at a critical Rayleigh number, Ra_c, two-dimensional corotating rolls start to appear in the flow. The stability of the two-dimensional rolls was examined confronting the linear predictions with the nonlinear integration. It was demonstrated that the two-dimensional rolls are always destabilized in the spanwise direction. The linear stability analysis revealed a competition between two eigenmodes which correspond to different spanwise wavelengths and distortion types of the rolls respectively. It was further found by a nonlinear integration operation that the lower-wave-number mode is always dominant. It was, however, interesting to find that the flow becomes temporally chaotic at $Ra = 1.05\,Ra_c$. Nevertheless, it can still be characterized by the spatial patterns identified by the linear stability analysis.

The stability of a two-dimensional free convection flow in a square cavity with the presence of a uniform internal heat source and a uniform magnetic field was investigated with linear stability analysis by Pelekasis [16]. The finite element method was employed to obtain the steady and dynamic states of flow while linear stability analysis was carried out by solving a generalized eigenvalue problem. It was shown from

*yang.liu1@qq.com or yangliu1@dlut.edu.cn

the base solution that two recirculation regions exist when the heat production term is amply high. The Hopf bifurcation was identified through the stability analysis, and a neutral stability map was further obtained for a wide range of flow parameters. It was also demonstrated that as the Grashof number increases, the two rolls vanish and the steady flow configuration becomes unstable when Gr increases beyond a critical number.

A similarity study has also been utilized to study the convective boundary layer flows. The similarity solutions of the energy equation are naturally applicable for the isothermal heating condition and constant heat flux forcing. The hydrodynamics of thermal boundary layers adjacent to a plate subject to the convective surface boundary condition was further examined and investigated with this approach by Aziz [17]. It is demonstrated that a similarity solution is possible if the heat transfer of the lower surface of the heated plate is proportional to $x^{-1/2}$ where x is the streamwise location from the leading edge. This finding was recently confirmed by Ishak [18]. The similarity energy equation was eventually obtained for various Prandtl numbers and Rayleigh numbers by Aziz [17].

The convective flow and the associated heat transfer over a horizontal flat plate were analytically investigated with local similarity and local nonsimilarity methods by Chen *et al.* [19]. Numerical results of the local Nusselt number, velocity, and temperature profiles were obtained for a fluid with a Prandtl number (Pr) of 0.7. It was found that the local Nusselt number increases with the buoyancy force for aiding flow, and it decreases with the buoyancy force for opposing flow. Significant buoyancy effects were seen at $\mathrm{Gr}_x/\mathrm{Re}_x{}^{5/2} < -0.03$ and $\mathrm{Gr}_x/\mathrm{Re}_x{}^{5/2} > 0.05$ for aiding and opposing flows, respectively. Overshoot behavior was observed in the velocity profile in the aiding-flow scenario. The authors suggested that their results agree well with previous solutions only when the buoyancy effects are small.

The so-called scaling analysis obtains the interdependency of various flow variables on the governing parameters of the flow problem by comparing the force and energy terms in the governing equations. This methodology has been proven to be especially useful for investigations of the buoyancy-driven convective flows since it was first proposed by Patterson and Imberger [20]. In this landmark work, the convective flow in a cavity was studied with a $\mathrm{Pr} > 1$ fluid where several possible flow regimes were proposed, and the scales describing the thermal boundary layer flow, intrusion flow, and the interior potential flow were obtained.

In recent decades, Lin and his coworkers have been consistently and rigorously improving this method and have intensively utilized this method to analyze various convective flows. The long-term behavior of cooling an initially quiescent isothermal Newtonian fluid in a rectangular container was investigated by scaling analysis and direct numerical simulation (DNS) by Lin and Armfield [21]. Two thermal configurations were considered by the authors. Later Lin *et al.* [22] further investigated the convective flow of $\mathrm{Pr} < 1$ fluids with the scaling analysis approach, and various scales quantifying the $\mathrm{Pr} < 1$ fluids were obtained. After revisiting the $\mathrm{Pr} > 1$ fluid flows, Lin *et al.* [23] successfully considered the effect of Prandtl number by separately studying the three regions of the boundary layer flow. Up to 2012, this methodology has been successfully applied to quantify the $\mathrm{Pr} > 1$ and $\mathrm{Pr} < 1$ fluids. However, it cannot describe fluids with $\mathrm{Pr}\sim 1$. To tackle this issue, Lin and Armfield [24] proposed sets of unified scaling law to describe both the $\mathrm{Pr} \lesssim 1$ and $\mathrm{Pr} \gtrsim 1$ fluids mainly by fitting their DNS-obtained results. Apart from the homogenously isothermal forcing, the uniform heating condition was also studied with the scaling analysis by Lin and Armfield [25,26].

The above literature review implies that the convective boundary layer flow subject to linear thermal forcing has been much less investigated, and the corresponding underlying dynamics were also not well understood. This heating configuration is worth a comprehensive scaling analysis since this is also frequently encountered in various industrial applications, such as the cooled surface of a domestic fridge and the water feed pipe in an ocean thermal energy conversion plant. The thermal boundary layer induced by heating a linear stratified fluid was primarily investigated in Ref. [27]. In a recent paper, Liu *et al.* [28] successfully scaled the thermal boundary layer flow and the subsequent intrusion flow in a differentially and linearly heated cavity. Nevertheless, the specified linear thermal forcing requires the temperature difference at the leading edge location to be zero. Therefore, the obtained scales were in fact not quite generalized and cannot be easily extended to other convective flows since there are many situations in which the boundary layer grows from a nonzero temperature difference. This motivates the present study.

In this paper, a scaling analysis is carefully carried out for the transient convective boundary layer flow where the effects of Rayleigh number, Prandtl number, streamwise location, background temperature stratification, and evolutionary time are all considered. It is worth clarifying that the local temperature difference at the leading edge location can be any desirable value by properly specifying the temperature stratification factor. It is also worth noting that both the $\mathrm{Pr} < 1$ and $\mathrm{Pr} > 1$ fluids are analyzed in the present work.

As a reminder of this paper, the physical problem and the adopted DNS approach are stated in Sec. II. Section III presents the scaling analysis for both the $\mathrm{Pr} < 1$ and $\mathrm{Pr} > 1$ fluids followed by numerical validations in Sec. IV. Section V summarizes the main findings.

II. PROBLEM FORMULATION

A. Physical problem

Under consideration is a transient convective boundary layer flow induced by a heated semi-infinite vertical plate. At time $\tau < 0$, the ambient fluid is at rest and its temperature is the same as that of the plate, θ_0. At $\tau = 0$, the wall is suddenly heated and the convective flow is subsequently initiated.

A schematic of the investigated model is sketched in Fig. 1(a). The left surface of the model is the heated semi-infinite vertical plate, and the other three boundaries are open. It is noted that to ensure the employed boundaries do not affect the flow parameters of interest to the present study, an additional model with an extended region of a length $0.2h$ at the upstream of the domain was also examined. The

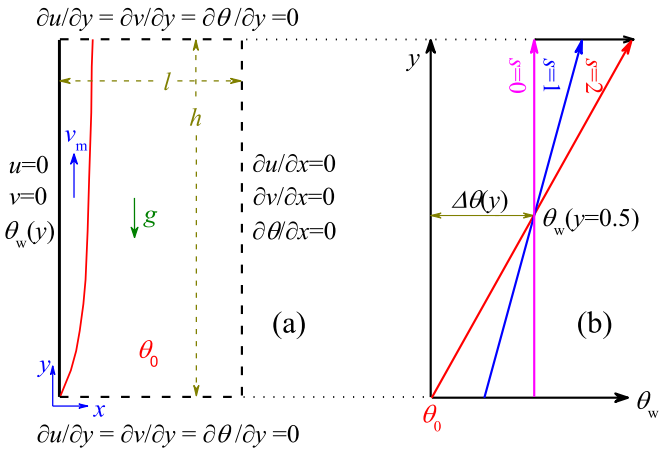

FIG. 1. Schematic of employed model. (a) Heated semi-infinite vertical plate; (b) Temperature profile of the heated semi-infinite plate.

corresponding results compared well with the data obtained from the present one as depicted in Fig. 1(a). Considering the computing cost, the domain without the upstream extension is hence utilized.

In the present study, a linear thermal forcing is imposed at the semi-infinite plate where a temperature stratification factor is defined as $s = d\theta_w(y)/dy$. Here $\theta_w(y)$ is the local temperature at a streamwise location of y of the heated surface, shown in Fig. 1(b).

Apart from the temperature stratification factor, s, the Rayleigh number, Prandtl number, and aspect ratio of the model also govern the present flow. They are defined as

$$\mathrm{Ra} = \frac{g\beta\Delta T H^3}{\nu\kappa}, \tag{1}$$

$$\mathrm{Pr} = \frac{\nu}{\kappa}, \tag{2}$$

$$A = \frac{H}{L}, \tag{3}$$

where g, β, ν, and κ are the gravitational acceleration, thermal expansion coefficient, kinematic viscosity, and thermal diffusivity of the working fluid, respectively. H and L are the equivalent dimensional height and length of the model. Aspect ratio of the employed model is fixed at 2. ΔT is the equivalent dimensional temperature difference at $y = 0.5$, which corresponds to $\Delta T = T_w(0.5H) - T_0$. It is noted that the ΔT is fixed in the present study regardless of Ra, Pr, and s utilized.

B. Numerical settings

The flow is accounted for by means of DNS in the present study. The governing equations are the two-dimensional Navier-Stokes equations with the Boussineq approximation for buoyancy along with the continuity and energy conservation equations. A fluctuating temperature is defined as $\theta_\mathrm{f}(x, y) = \theta(x, y) - \theta_\mathrm{w}(y)$ in this study. Then the governing equations can be expressed as

$$\frac{\partial u}{\partial x} + \frac{\partial v}{\partial y} = 0, \tag{4}$$

$$\frac{\partial u}{\partial \tau} + u\frac{\partial u}{\partial x} + v\frac{\partial u}{\partial y} = -\frac{\partial p}{\partial x} + \frac{\mathrm{Pr}}{\mathrm{Ra}^{1/2}}\left(\frac{\partial^2 u}{\partial x^2} + \frac{\partial^2 u}{\partial y^2}\right), \tag{5}$$

$$\frac{\partial v}{\partial \tau} + u\frac{\partial v}{\partial x} + v\frac{\partial v}{\partial y} = -\frac{\partial p}{\partial y} + \frac{\mathrm{Pr}}{\mathrm{Ra}^{1/2}}\left(\frac{\partial^2 v}{\partial x^2} + \frac{\partial^2 v}{\partial y^2}\right) + \mathrm{Pr}\Delta\theta_f, \tag{6}$$

$$\frac{\partial \theta_f}{\partial \tau} + u\frac{\partial \theta_f}{\partial x} + v\frac{\partial \theta_f}{\partial y} + vs = \frac{1}{\mathrm{Ra}^{1/2}}\left(\frac{\partial^2 \theta_f}{\partial x^2} + \frac{\partial^2 \theta_f}{\partial y^2}\right). \tag{7}$$

The flow parameters are nondimensionalized by

$$x = \frac{X}{H}, \quad y = \frac{Y}{H}, \quad u = \frac{U}{U_0}, \quad v = \frac{V}{U_0}, \quad p = \frac{P}{\rho {U_0}^2},$$
$$\tau = \frac{t}{H/U_0}, \quad \theta = \frac{T - T_w(0.5H)}{\Delta T}, \tag{8}$$

where the lower and upper letters denote dimensionless and dimensional variables, respectively. U_0 is the velocity scale proposed by Patterson and Imberger [20] and it equals $\kappa \mathrm{Ra}^{1/2}/H$.

Hence, the local temperature at the semi-infinite vertical plate can be calculated by

$$\theta_w(y) = s(y - 0.5). \tag{9}$$

It is seen in Fig. 1(b) that the local temperature difference at the leading edge of the thermal boundary layer can be a nonzero value, which makes the present study distinctly different from previous similar investigations (see, e.g., Refs. [22,28–30]). It is also known that the fluctuating temperature along the heated semi-infinite vertical plate is reduced to zero considering $\theta_f(x, y) = \theta(x, y) - \theta_w(y)$, and the difference in the local fluctuating temperature can be calculated by $\Delta\tilde{\theta}_f(y) = 1 - s(0.5 - y)$. It is worth clarifying that $\Delta\tilde{\theta}_f(y)$ denotes the difference of fluctuating temperature over the boundary layer thickness (which is in the x direction) at a streamwise location of y. It is thus reduced to being one-dimensional, i.e., it depends only on y. It is also noted in Eq. (6) that the $\Delta\theta_\mathrm{f}$ corresponds to the fluctuating temperature difference, which is in relation to the fluctuating temperature of θ_0, i.e., θ_{f0}. Hereby, we have $\Delta\theta_f = \theta_f - \theta_{f0}$. It is also worth noting that the flow reduces to the traditional homogenously heating problem when $s = 0$.

The governing equations are implicitly solved with a finite volume method algorithm. The advection terms are discretized by the QUICK scheme. The spatial discretization of all second-derivative terms and linear first-derivative terms adopts the second-order central-differenced scheme [31]. The transient term uses a second-order backward difference method. A pressure correction-based iterative algorithm, SIMPLE, was used during the computations [32]. The solution is converged when the scaled residual of the computational cell falls below 10^{-6} for the temperature equation and 10^{-3} for the

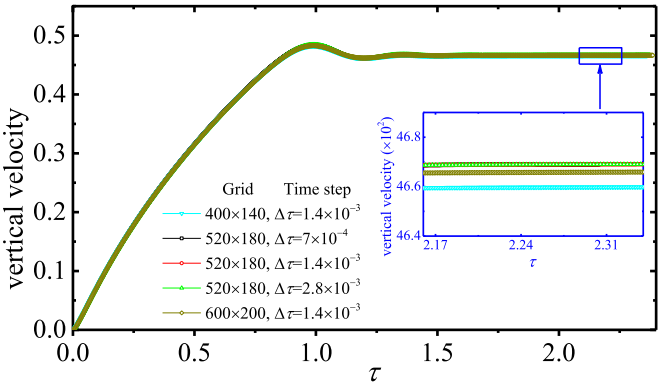

FIG. 2. Time series of vertical velocity at the monitoring point ($x = 0.004$, $y = 0.5$) for grid- and time-step-dependency tests (Ra $= 1 \times 10^9$, Pr $= 100$, and $s = 0$).

continuity and momentum equations. The adopted numerical settings are similar to those adopted in Refs. [7,28].

Three grids and three time steps are examined to ensure the DNS-obtained results do not depend on these numerical arrangements. The constructed mesh systems are nonuniform, and the grid is finer towards the heated plate. During the calculations, the time series of the vertical velocity in the thermal boundary layer at a monitoring point ($x = 0.004$, $y = 0.5$) is recorded with the case Ra $= 1 \times 10^9$, Pr $= 100$, and $s = 0$. It needs to clarify that this specific case employed for the grid- and time-step-dependency tests corresponds to the "strongest" flow under investigation. The corresponding results are presented in Fig. 2.

It is found that the monitored parameter varies only slightly among different meshes and time steps, suggesting any combination can be adopted for the numerical calculations. Considering the computing efficiency, the grid system of 520×180 and the time step of 1.4×10^{-3} are employed for the following DNS calculations.

In the present study, both Pr < 1 and Pr > 1 fluids are investigated, and a total of 20 DNS runs are carried out to validate the derived scales. Detailed information of the calculated cases is listed in Table I. It is worth clarifying that only non-negative s is considered in the current study, $s \geqslant 0$. Also, to make sure the temperature at the heated semi-infinite plate is no lower than the ambient fluid, it then requires a non-negative fluctuating temperature at $y = 0$, $\Delta\tilde{\theta}_f(y = 0) \geqslant 0$. This subsequently requires $s \leqslant 2$. Therefore, the temperature stratification factor s ranges from 0 to 2 in this study as demonstrated in Fig. 1(b).

III. SCALING ANALYSIS

The convective boundary layer flow can be predominantly characterized by a thickness scale and a velocity scale. In the following sections, scaling analysis is carried out for various flow conditions and fluid properties, which will lead to comprehensive understanding and scales of the convective boundary layer at both the start-up and the fully developed states. It is worth noting that the present work differentiates from the previous ones (see, e.g., Refs. [20,23]) in adopting a linear temperature gradient at the heated surface.

A. Pr > 1 fluids

Immediately after the initiation of the convective flow, heat is conducted into the interior fluid, and this subsequently results in a thermal boundary layer flow adjacent to the heated plate. In this process, the unsteady term in the energy conservation equation, or the so-called inertial term, is very large. Hence, the ratio of the unsteady term $\Delta\tilde{\theta}_f(y)/\tau$ to the convection term $v(\Delta\tilde{\theta}_f(y)/y + s)$ is much larger than unity. It is also noted that dimensions of the boundary layer are usually approximated by δ_θ and h in the x and y directions, respectively. Thus we have $\partial/\partial x \sim 1/\delta_\theta$, which is much larger than $\partial/\partial y \sim 1/h$ in the present study. Therefore, the thermal balance of the boundary layer is between the inertial term and the diffusion term, which can be expressed as

$$\frac{\Delta\tilde{\theta}_f(y)}{\tau} \sim \frac{\Delta\tilde{\theta}_f(y)}{\mathrm{Ra}^{1/2}{\delta_\theta}^2}. \tag{10}$$

Then the scale of the thickness of the thermal boundary at the start-up state, δ_θ, can be obtained as

$$\delta_\theta \sim \mathrm{Ra}^{-1/4}\tau^{1/2}. \tag{11}$$

To precisely account for the effect of the Prandtl number, Lin *et al.* [23] suggested that the three-region structure of the thermal boundary layer needs to be considered and treated ingeniously. The corresponding profiles are illustrated in Fig. 3,

TABLE I. Detailed information of the 20 calculated case runs.

Run no.	Scenarios	s	Ra	Pr
1	Pr > 1	0	1×10^9	6.63
2		0.5	1×10^9	6.63
3–8		1	1×10^7, 5×10^7, 1×10^8, 1×10^9	6.63, 50, 100
9		1.5	1×10^9	6.63
10		2	1×10^9	6.63
11	Pr < 1	0	1×10^8	0.05
12		0.5	1×10^8	0.05
13–18		1	1×10^6, 1×10^7, 1×10^8	0.05, 0.1, 0.2, 0.5
19		1.5	1×10^8	0.05
20		2	1×10^8	0.05

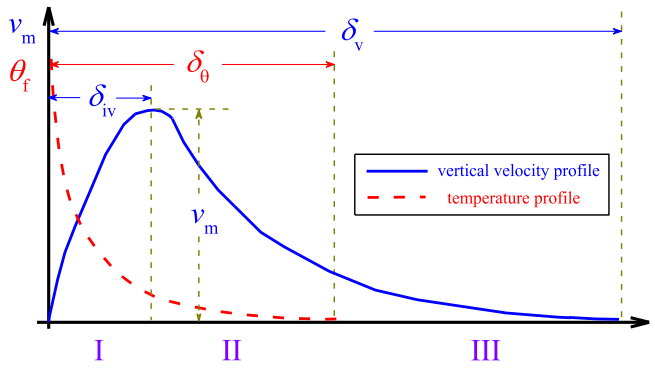

FIG. 3. Schematic of the three-region structure of boundary layer flow with Pr > 1.

which consists of an inner viscous layer, a thermal layer, and an outer viscous layer for the Pr > 1 fluids.

Region I corresponds to the inner viscous layer, and it is from the semi-infinite vertical plate to the horizontal location of the maximum vertical velocity. The width of this region is δ_{iv}. Buoyancy is the driving force in this region. In the vertical momentum, Eq. (6), the ratio of the inertial term $(\partial v/\partial\tau)$ to the viscous term $[\mathrm{Ra}^{-1/2}\mathrm{Pr}(\partial^2 v/\partial x^2)]$ is $1/\mathrm{Pr}$. This suggests that, for fluids with Pr > 1, the viscous term is greater than the inertial term. Then the inertial term can be ignored in this scenario, and we can write

$$\frac{\mathrm{Pr}v_m}{\mathrm{Ra}^{1/2}{\delta_{iv}}^2} \sim \mathrm{Pr}\Delta\tilde{\theta}_f(y). \tag{12}$$

Then we can come to a scale of the v_m as

$$v_m \sim \mathrm{Ra}^{1/2}\Delta\tilde{\theta}_f(y){\delta_{iv}}^2. \tag{13}$$

In region II the flow is not directly driven by buoyancy, and the corresponding motion is in fact caused by the diffusion of momentum. Therefore, considering the inertial term can be ignored, by integrating the vertical momentum equation over this region, we have

$$\frac{\mathrm{Pr}}{\mathrm{Ra}^{1/2}}\left(\frac{\partial v}{\partial x}\right)_{\delta_{iv}}^{\delta_\theta} \sim \mathrm{Pr}\int_{\delta_{iv}}^{\delta_\theta}\Delta\tilde{\theta}_f(y)dx. \tag{14}$$

It is worth clarifying for the right-hand side of Eq. (14) that the buoyancy vanishes beyond $x \sim \delta_\theta$. However, it is significant at $x \sim \delta_{iv}$. Thus the correct way to estimate the buoyancy over region II is to integrate. Considering that $(\frac{\partial v}{\partial x})_{\delta_{iv}} = 0$, $(\frac{\partial v}{\partial x})_{\delta_\theta} \approx \frac{v_m}{\delta_v - \delta_{iv}}$ and the difference in local fluctuating temperature, $\Delta\tilde{\theta}_f(y)$, is independent of x. Equation (14) can be rewritten as

$$\frac{\mathrm{Pr}}{\mathrm{Ra}^{1/2}}\frac{v_m}{\delta_v - \delta_{iv}} \sim \mathrm{Pr}\Delta\tilde{\theta}_f(y)\int_{\delta_{iv}}^{\delta_\theta} dx\,. \tag{15}$$

Hence the scale of the vertical velocity v_m is obtained as

$$v_m \sim \mathrm{Ra}^{1/2}\Delta\tilde{\theta}_f(y)(\delta_\theta - \delta_{iv})(\delta_v - \delta_{iv})\,. \tag{16}$$

Combining Eqs. (13) and (16), we have

$$(\delta_\theta - \delta_{iv})(\delta_v - \delta_{iv}) \sim {\delta_{iv}}^2. \tag{17}$$

In region III of the boundary layer, there is no temperature gradient implying the absence of buoyancy. In this region, the inertial term balances the viscous term. We can hence write

$$\frac{v}{\tau} \sim \frac{\mathrm{Pr}}{\mathrm{Ra}^{1/2}}\frac{v}{{\delta_v}^2}. \tag{18}$$

Then we can obtain the thickness of the outer viscous layer as

$$\delta_v \sim \mathrm{Pr}^{1/2}\delta_\theta. \tag{19}$$

By substituting Eq. (19) into Eq. (17), we can come to the scale quantifying the thickness of the inner viscous layer as

$$\delta_{iv} \sim \frac{\delta_\theta\delta_v}{\delta_\theta + \delta_v} \sim \frac{\delta_\theta}{1 + \mathrm{Pr}^{-1/2}} \sim \frac{\tau^{1/2}}{\mathrm{Ra}^{1/4}(1 + \mathrm{Pr}^{-1/2})}. \tag{20}$$

The scale of v_m at the start-up state can be obtained by inserting Eq. (20) into Eq. (13) as

$$v_m \sim \frac{\Delta\tilde{\theta}_f(y)\tau}{(1 + \mathrm{Pr}^{-1/2})^2} \sim \frac{[1 - s(0.5 - y)]\tau}{(1 + \mathrm{Pr}^{-1/2})^2}. \tag{21}$$

The boundary layer thickens in the initial growth state until a time instance at which the heat conducted in through the heated plate is completely convected away by the boundary layer. In Eq. (7), this corresponds to

$$v_m\left[\frac{\Delta\tilde{\theta}_f(y)}{y} + s\right] \sim \frac{1}{\mathrm{Ra}^{1/2}}\left[\frac{\Delta\tilde{\theta}_f(y)}{\delta_\theta^2}\right]. \tag{22}$$

This gives a timescale of τ_{sy} as

$$\tau_{sy} \sim \frac{(1 + \mathrm{Pr}^{-1/2})y^{1/2}}{(1 - 0.5s + 2sy)^{1/2}}. \tag{23}$$

Combining Eqs. (21) and (23), the scale of the characteristic velocity of the steady-state boundary layer is obtained as

$$v_{msy} \sim \frac{(1 - 0.5s + sy)y^{1/2}}{(1 + \mathrm{Pr}^{-1/2})(1 - 0.5s + 2sy)^{1/2}}. \tag{24}$$

By substituting Eq. (23) into Eq. (11), the thickness of the steady-state boundary layer is obtained as

$$\delta_{\theta sy} \sim \frac{(1 + \mathrm{Pr}^{-1/2})^{1/2}y^{1/4}}{\mathrm{Ra}^{1/4}(1 - 0.5s + 2sy)^{1/4}}. \tag{25}$$

Insert Eq. (23) into Eq. (20), and we can come to the scale quantifying the thickness of the steady-state inner viscous boundary layer as

$$\delta_{ivs} \sim \frac{y^{1/4}}{\mathrm{Ra}^{1/4}(1 + \mathrm{Pr}^{-1/2})^{1/2}(1 - 0.5s + 2sy)^{1/4}}. \tag{26}$$

B. Pr < 1 fluids

The boundary layer flow associated with Pr < 1 fluids will be analyzed in the present section. It is worth clarifying at this point that, unlike the Pr > 1 fluids, the effect of Prandtl number of Pr < 1 fluids can be reasonably quantified without examining the near-wall flow and thermal profiles [22].

When the thermal forcing is applied at the heated semi-infinite vertical plate, the convective flow is immediately initiated. In the energy conservation, Eq. (7), the inertial term is $\Delta\tilde{\theta}_f(y)/\tau$, the advection term is $v(\Delta\tilde{\theta}_f(y)/y + s)$ and the thermal diffusion term is $\Delta\tilde{\theta}_f(y)/\mathrm{Ra}^{1/2}{\delta_\theta}^2$. The ratio of

inertial term to advection is greater than one when the time is small enough, and the advection term therefore can be ignored on this occasion. We can hereby obtain the thickness of the thermal boundary layer in the start-up state as

$$\delta_\theta \sim \mathrm{Ra}^{-1/4}\tau^{1/2}. \tag{27}$$

Consider the vertical momentum Eq. (6), the inertial term is v/τ, the advection term is v^2/y, the viscous term is $\mathrm{Pr}v/\mathrm{Ra}^{1/2}{\delta_\theta}^2$, and the buoyancy term is $\mathrm{Pr}\,\Delta\tilde{\theta}_f(y)$. The ratio of inertial term to the advection term is $y/\tau v$, which is higher than the unity immediately after the initiation of the flow. Therefore for the $\mathrm{Pr} < 1$ fluids, the correct balance should be between the inertial, viscous, and buoyancy forces, as suggested by Lin *et al.* [22]:

$$\frac{v_m}{\tau} + \frac{\mathrm{Pr}}{\mathrm{Ra}^{1/2}}\frac{v_m}{\delta_\theta^2} \sim \mathrm{Pr}\Delta\tilde{\theta}_f(y)\,. \tag{28}$$

Hence, the scale of the velocity of the thermal boundary layer at the developing state can be obtained as

$$v_m \sim \frac{\Delta\tilde{\theta}_f(y)\tau}{(1+\mathrm{Pr}^{-1})}\,. \tag{29}$$

The boundary layer will keep growing until the convection balances the conduction. We can find this balancing in the energy equation by

$$v_m\left[\frac{\Delta\tilde{\theta}_f(y)}{y} + s\right] \sim \frac{1}{\mathrm{Ra}^{1/2}}\left[\frac{\Delta\tilde{\theta}_f(y)}{\delta_\theta^2}\right]. \tag{30}$$

Then we can come to the timescale τ_{sy} beyond which the boundary layer will transit to a steady state:

$$\tau_{sy} \sim \frac{(1+\mathrm{Pr}^{-1})^{1/2}y^{1/2}}{(1-0.5s+2sy)^{1/2}}. \tag{31}$$

By inserting Eq. (31) into Eqs. (27) and (29), we can obtain the scales quantifying the velocity and thickness of the steady-state boundary layer as

$$v_{msy} \sim \frac{(1-0.5s+sy)y^{1/2}}{(1+\mathrm{Pr}^{-1})^{1/2}(1-0.5s+2sy)^{1/2}}, \tag{32}$$

$$\delta_{\theta sy} \sim \frac{(1+\mathrm{Pr}^{-1})^{1/4}y^{1/4}}{\mathrm{Ra}^{1/4}(1-0.5s+2sy)^{1/4}}. \tag{33}$$

IV. VALIDATION OF THE DERIVED SCALES

A. Pr > 1 fluids

Figure 4(a) presents time histories of the normalized temperature in the convective boundary layer adjacent to the heated semi-infinite vertical plate for the case with a Rayleigh number of 1×10^9 and a Prandtl number of 6.63. The initial growth, transitional state, and eventual steady state are all clearly revealed. It is also demonstrated in this figure that the temperature oscillatory behavior and the temperature overshoot phenomenon greatly depend on the specified stratification factor. When it equals zero, i.e., when $s = 0$, the thermal condition is reduced to the extensively investigated homogenously heating problems, and this corresponds to the strongest leading edge effect (LEE). It is interesting to note that the temperature overshoot is barely seen at $s = 2$.

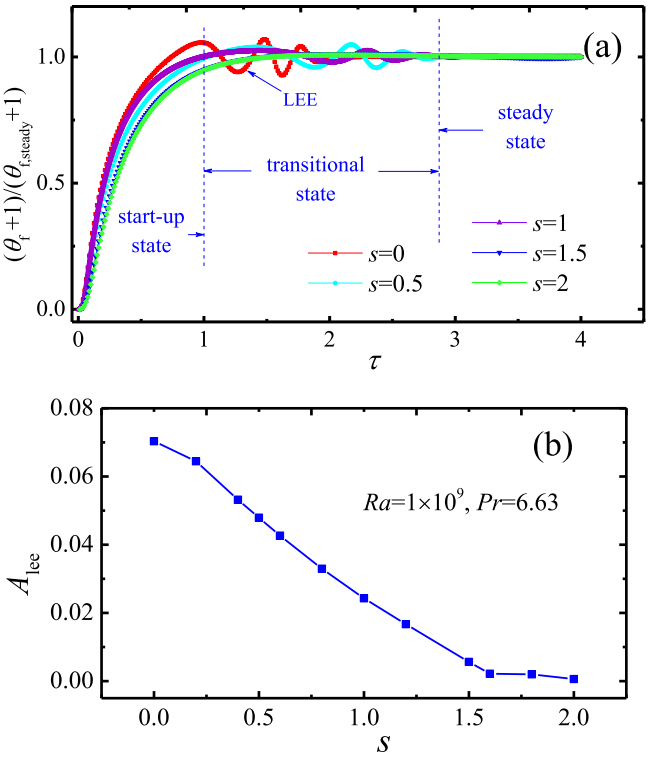

FIG. 4. Normalized temperature-time series at the monitoring point ($x = 0.004$, $y = 0.5$) with $\mathrm{Ra} = 1 \times 10^9$ and $\mathrm{Pr} = 6.63$.

Figure 4(b) shows the amplitude of the temperature oscillation in the transitional state to primarily reveal the effect of temperature stratification on LEE. It is seen that A_{lee} monotonically decreases with s, and it reduces to approximately zero at $s = 2$. As discussed in Sec. II, the difference of the local fluctuating temperature is $\Delta\tilde{\theta}_{\mathrm{f}}(y) = 1 - s(0.5 - y)$. At the leading edge location, $y = 0$, the temperature difference becomes zero if s equals to 2. This suggests that the LEE and the subsequent traveling waves are the weakest if the temperature difference at the leading edge equals to zero. This is consistent with our ongoing studies, and our previous work for the $\mathrm{Pr} > 1$ fluid also exhibits the same behavior. However, it is also seen that A_{lee} does not significantly change with the stratification factor when s is above approximately 1.6. The corresponding investigation might be carried out in a further separate study since the present work mainly focuses on the scaling laws of the transient convective boundary layer flow.

Figure 5(a) presents profiles of normalized temperature obtained with various stratification factors, times, Prandtl numbers, and streamwise locations at the start-up state. It is seen that the temperature decreases gradually towards the interior fluid. It is also clear in this figure that the thickness of the thermal boundary layer does vary among these parameters. Figure 5(b) plots the normalized temperature against $x/\tau^{1/2}$ at the specific Rayleigh number of 1×10^9. It is seen in Fig. 5(b) that all data fall onto approximately the same line, suggesting the proposed scale in Eq. (11) can accurately describe the thickness of the thermal boundary layer in the initial growth state. It is also worth noting that the legend of

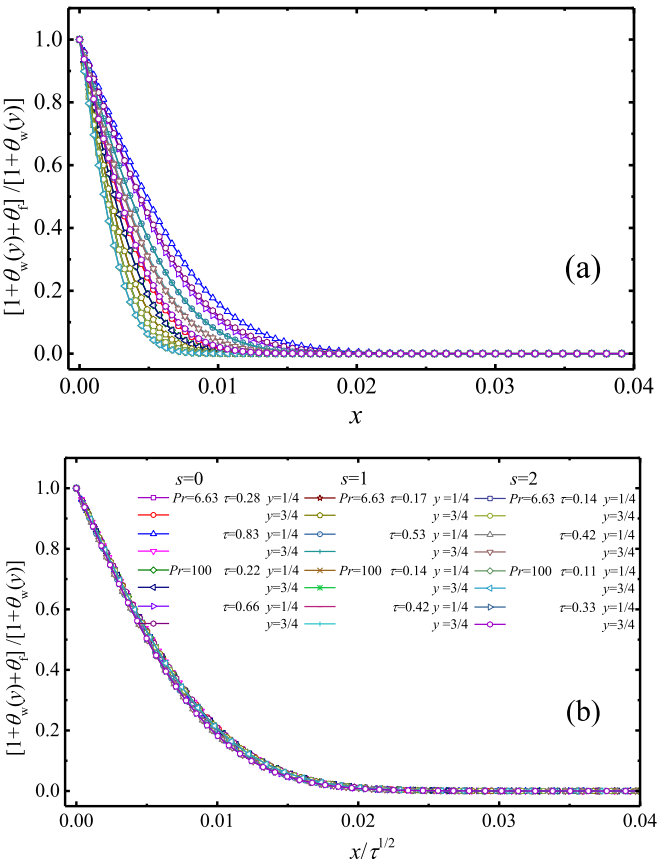

FIG. 5. Profiles of normalized temperature adjacent to the heated plate at the start-up state. ($\mathrm{Ra} = 1 \times 10^9$). (a) Raw data; (b) Normalized temperature against $x/\tau^{1/2}$.

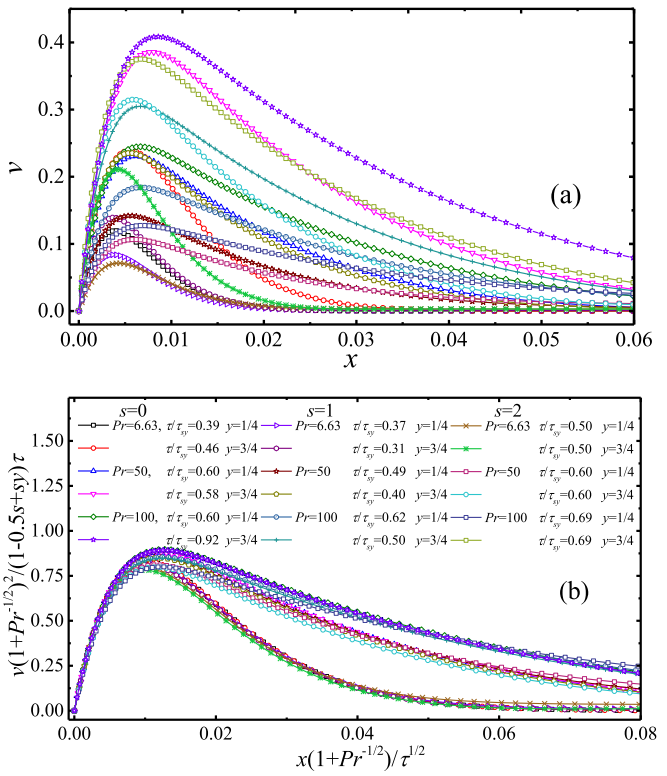

FIG. 6. Velocity profiles of convective boundary layer at the start-up state. ($\mathrm{Ra} = 1 \times 10^9$). (a) Raw data; (b) Normalized velocity $v(1+\mathrm{Pr}^{-1/2})^2/(1-0.5s+sy)\tau$ vs $x(1+\mathrm{Pr}^{-1/2})/\tau^{1/2}$.

Fig. 5 is inserted only in Fig. 5(b) for conciseness, and the same procedure is adopted for Figs. 6 and 8.

Figure 6(a) presents the velocity profiles obtained with various stratification factors, times, Prandtl numbers, and streamwise locations at the start-up state. It is seen from the raw data in Fig. 6(a) that the maximum velocity is different case by case, and it is also found that the velocity maximizes at different horizontal locations, suggesting the thickness of the inner viscous boundary layer also greatly depends on these flow parameters. Figure 6(b) shows the normalized velocity of $v(1+\mathrm{Pr}^{-1/2})^2/(1-0.5s+sy)\tau$ against $x(1+\mathrm{Pr}^{-1/2})/\tau^{1/2}$ at the specific Rayleigh number of 1×10^9. It is seen in Fig. 6(b) that all data within the inner viscous boundary layer collapse onto approximately the same line, suggesting the proposed scales in Eqs. (20) and (21) can properly quantify the thickness and momentum of the boundary layer flow at the start-up state.

Convection becomes more important with the increase of time, and the boundary layer transits to a steady state when the convection is comparable with the conduction. The thickness of the thermal boundary layer is monitored and recorded at different Rayleigh numbers, Prandtl numbers, times, stratification factors, and streamwise locations during the DNS computations. The corresponding thickness time series are presented in Fig. 7. It is demonstrated that the thermal boundary layer thickens with time in the developing state according to $(\tau/\tau_{\mathrm{sy}})^{1/2}$. At $\tau \sim \tau_{\mathrm{sy}}$ the thickness starts to overshoot, and the oscillatory behaviors are seen in the transitional state. The boundary layer eventually reaches a steady state after the passage of the LEE phenomenon. It is also clear that, apart from the temperature oscillations caused by the LEE in the transitional state, all data points fall onto approximately the same line supporting Eqs. (11) and (23). Note that the thickness of the thermal boundary layer is identified at the location where the temperature equals 5% of the local fluctuating temperature difference in the present DNS calculations. Our separate study shows that the agreement between DNS calculations and scaling is not affected if another criterion of identifying the boundary layer edge was employed, e.g., 3% or 8%. It is also worth noting in Fig. 7 that

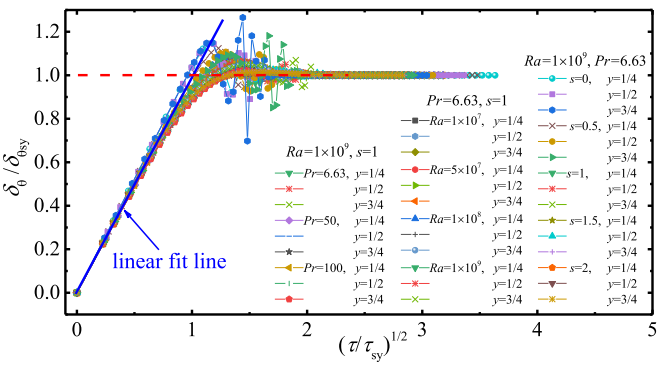

FIG. 7. DNS-obtained $\delta_\theta/\delta_{\theta sy}$ vs $(\tau/\tau_{sy})^{1/2}$.

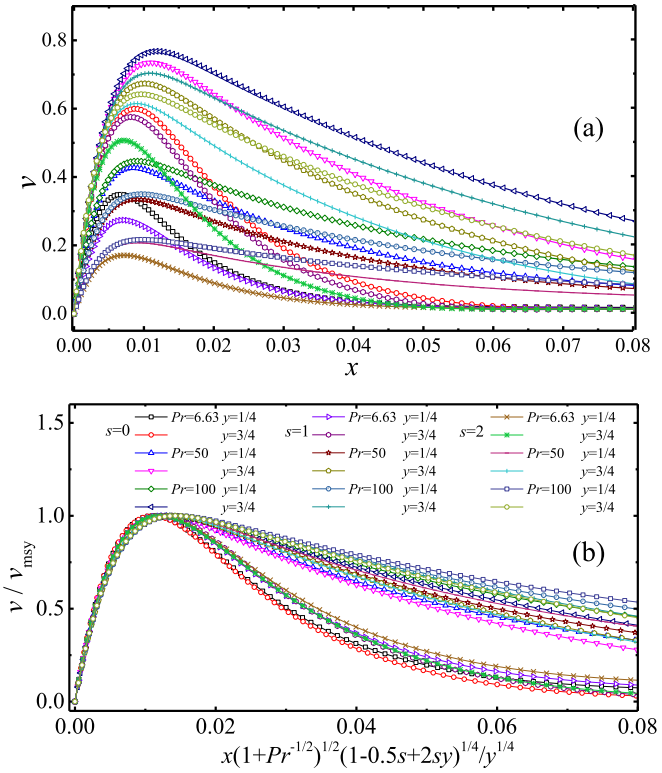

FIG. 8. Velocity profiles of boundary layer flow at the steady state ($\mathrm{Ra} = 1 \times 10^9$ at $\tau = 4.5\tau_{sy}$). (a) Raw data; (b) v/v_{msy} vs $x(1 + \mathrm{Pr}^{-1/2})^{1/2}(1 - 0.5s + 2sy)^{1/4}y^{1/4}$.

both the numerator and denominator appearing in the vertical axis are determined from the present DNS calculations, while the denominator appearing in the horizontal axis is calculated by the corresponding scaling relation. The same procedure is adopted for Figs. 9, 13, and 14 below.

It is seen in Fig. 7 that the thermal boundary layer fully stabilizes after approximately $4\tau_{\mathrm{sy}}$. The velocity profiles of the steady-state convective flow adjacent to the heated semi-infinite vertical plate at various Pr, s, y are plotted in Fig. 8(a). It is clearly demonstrated in this figure that the maximum velocity and the horizontal location which corresponds to the maximum velocity also depend on these parameters. The horizontal and vertical coordinates in Fig. 8(a) are further normalized by the thickness of the inner viscous layer and the

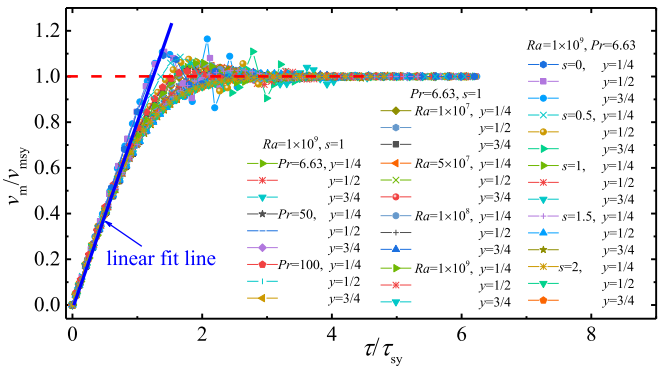

FIG. 9. Numerically obtained v_m/v_{msy} vs τ/τ_{sy}.

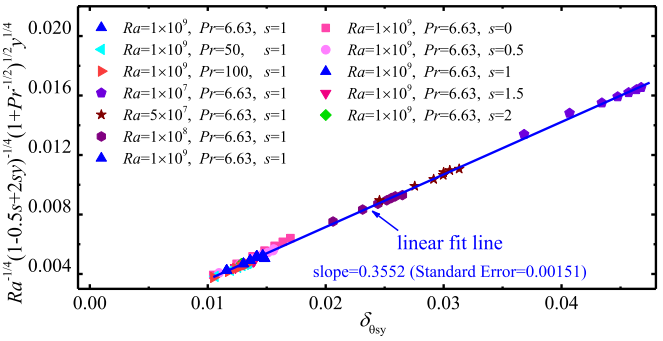

FIG. 10. Scale of $\mathrm{Ra}^{-1/4}(1 - 0.5s + 2sy)^{-1/4}(1 + \mathrm{Pr}^{-1/2})^{1/2}y^{1/4}$ vs numerically obtained $\delta_{\theta sy}$ at the steady state.

characteristic velocity of the boundary layer respectively in Fig. 8(b). It is seen that the velocity profiles within the inner viscous boundary layer almost collapse onto the same line, suggesting the proposed scale in Eq. (26) can well quantify the thickness of the viscous boundary layer at the steady state. It also needs to mention that v_{msy} as appears in the vertical axis of Fig. 8 is obtained from the present DNS calculations.

According to Eq. (21), the characteristic velocity of the thermal boundary layer increases with time according to $v_{\mathrm{m}} \sim \tau$. Note that the maximum vertical velocity within the boundary layer obtained from the present DNS calculation is taken to be its characteristic velocity, $v_{\mathrm{m}} = \max[v]$. This parameter is recorded during the computations, and Fig. 9 plots the time histories of the corresponding velocity ratio. The initial growth, transitional, and steady states as observed in Fig. 7 are also clearly demonstrated in Fig. 9. It is also seen that the results of velocity ratios obtained with different Ra, Pr, y, and s fall onto approximately the same line at both the initial growth and the steady states, suggesting the proposed scales in Eqs. (21) and (23) can appropriately describe the boundary layer flow.

Figure 10 presents the thickness of the steady-state thermal boundary layer obtained from the present DNS calculations against the scale of $\delta_{\theta sy}$, Eq. (25). Note that the presented results are obtained at different Ra, Pr, s, and y. A clear linear correlation is seen validating the corresponding scale. It is also seen that the scaling predictions slightly deviate from the numerical results with the $\mathrm{Ra} = 1 \times 10^7$ case. This corresponds to the lowest Rayleigh number studied at $\mathrm{Pr} > 1$. In this case the conduction becomes relatively important in relation to convection compared to higher Ra cases. Nevertheless, R^2 of the linear fit is found to be 0.99505, still validating the corresponding derived scale relation.

Figure 11 presents the numerically calculated velocity of the steady-state thermal boundary layer against the scale of v_{msy}, Eq. (24). The DNS results at different Ra, Pr, s, and y are shown in this figure. It is seen that the proposed scale can accurately describe the velocity in the boundary layer supporting the corresponding scale relation in Eq. (24).

The above analysis and validation show that the dynamics of the boundary layer flow is determined by the balances between the various terms of the governing equations. It is also demonstrated in Sec. III that for the fluids with $\mathrm{Pr} > 1$, the momentum of the boundary layer flow is dominated by the

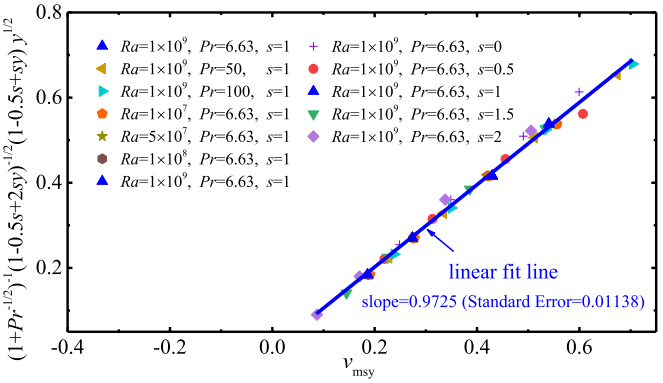

FIG. 11. Scale of $(1+\mathrm{Pr}^{-1/2})^{-1}(1-0.5s+2sy)^{-1/2}(1-0.5s+sy)y^{1/2}$ vs numerically obtained v_{msy} at the steady state.

buoyancy and the viscous effects while all other terms can be subsequently neglected. Figure 12(a) presents the horizontal profiles of the inertial, horizontal advection, vertical advection, viscous, buoyancy terms as well as the velocity of the convective boundary layer with the case $\mathrm{Ra} = 1 \times 10^8$, $\mathrm{Pr} = 6.63$, $s = 1$ at a streamwise location of 0.5 and a time instance of $0.22\tau_{\mathrm{sy}}$ (in the developing state). It is clearly seen that the buoyancy and viscous are indeed much more significant than the other terms in the initial growth state. Figure 12(b) further shows the profiles of these terms at a much later time, at

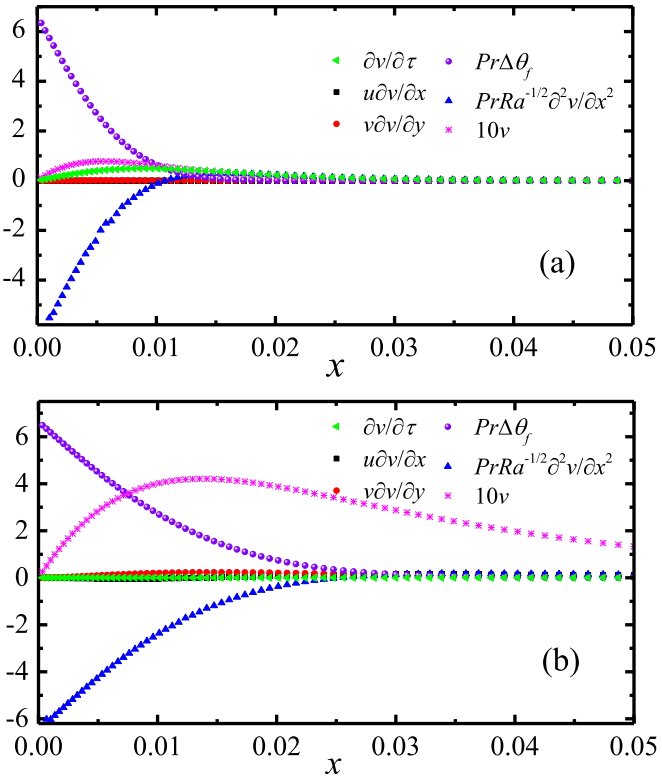

FIG. 12. Horizontal profiles of the unsteady term, horizontal advection term, vertical advection term, buoyancy term, viscous term, and velocity with the case $\mathrm{Ra} = 1 \times 10^8$, $\mathrm{Pr} = 6.63$, $s = 1$ at a streamwise location of $y = 0.5$. (a) Start-up state (at $\tau = 0.22\,\tau_{sy}$); (b) Steady state (at $\tau = 4.38\tau_{sy}$).

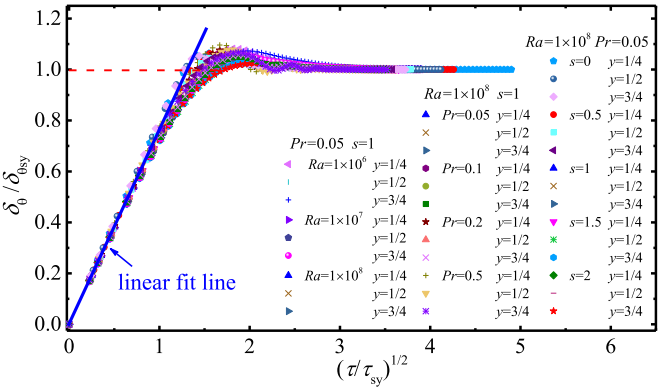

FIG. 13. DNS-obtained $\delta_\theta/\delta_{\theta sy}$ vs $(\tau/\tau_{sy})^{1/2}$.

$4.38\tau_{\mathrm{sy}}$ at which time the flow has transited to the steady state. It is also seen that values of all the other terms are much lower than the viscous and buoyancy. The growth in characteristic velocity and thickness of the convective boundary layer is also clearly demonstrated in these two figures. It is worth noting that the velocity profiles obtained from the present DNS calculations are timed by 10 to better demonstrate its growth with time in Figs. 12(a) and 12(b).

B. Pr < 1 fluids

Flows associated with the $\mathrm{Pr} < 1$ fluids are fundamentally different from the $\mathrm{Pr} > 1$ ones, and this is caused by the different underlying dynamics and force balances. It has been demonstrated in the present study that different sets of scale quantify the $\mathrm{Pr} < 1$ and $\mathrm{Pr} > 1$ flow. The scales describing the $\mathrm{Pr} < 1$ fluids will be validated in the present section.

Figure 13 plots the thickness ratio of the thermal boundary layer against $(\tau/\tau_{sy})^{1/2}$. The initial growth state, transitional state, and eventual steady state are all clearly seen in this figure. It also demonstrates that, apart from the transitional state which is affected by the LEE, all the DNS-obtained results converge onto approximately the same line supporting the scales in Eqs. (27) and (31).

Figure 14 plots the velocity ratio of the thermal boundary layer against τ/τ_{sy}. It is seen that the velocity increases with time according to $v_m \sim \tau$, and this is consistent with the scale relation in Eq. (29). Oscillations in velocity are also observed

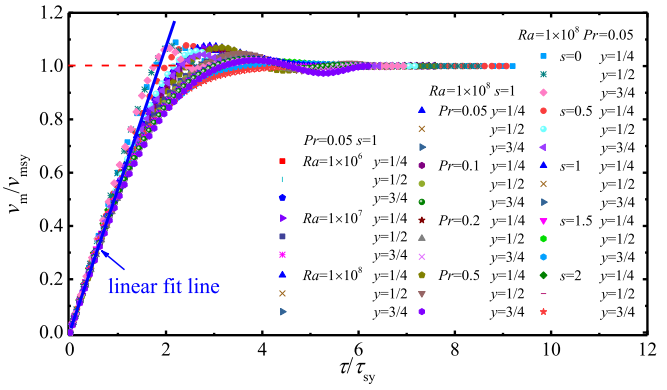

FIG. 14. DNS-obtained v_m/v_{msy} vs τ/τ_{sy}.

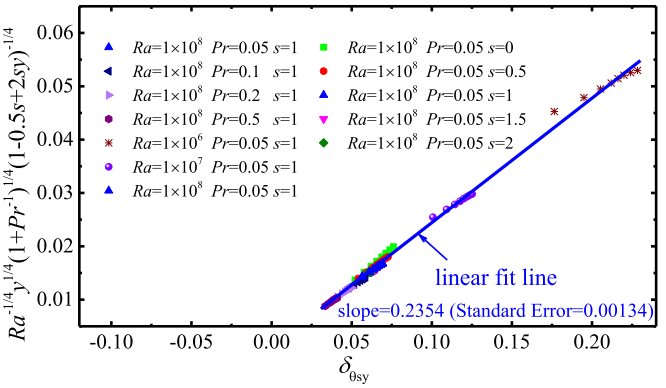

FIG. 15. Scale of $\mathrm{Ra}^{-1/4}y^{1/4}(1+\mathrm{Pr}^{-1})^{1/4}(1-0.5\mathrm{s}+2sy)^{-1/4}$ vs numerically obtained $\delta_{\theta sy}$ at the steady state.

in the transitional state, and it is associated with the LEE phenomenon. After the passage of the LEE-caused oscillatory behaviors, the boundary layer enters the steady state. It is also found in this figure that the numerically obtained data almost fall onto the same line in both the early and steady states.

The thickness of the steady-state thermal boundary layer obtained from the present DNS calculations is presented in Fig. 15 against the scale of $\mathrm{Ra}^{-1/4}y^{1/4}(1+\mathrm{Pr}^{-1})^{1/4}(1-0.5\mathrm{s}+2sy)^{-1/4}$. It is seen that the proposed scale in Eq. (33) can reasonably quantify the thickness of the steady-state boundary layer at different streamwise locations and at various working conditions. Deviation between scaling and numerical results is noticed with the $\mathrm{Ra}=1\times10^6$ case in this figure, which corresponds to the lowest Rayleigh number studied at $\mathrm{Pr}<1$. Similar to the aforementioned $\mathrm{Pr}>1$ case, this is in fact caused by the relative relation between conduction and convection. R^2 of the linear fit is found to be 0.98976, still supporting the corresponding derived scale relation.

Figure 16 presents the numerically calculated characteristic velocity of the steady-state thermal boundary layer against the scale of $(1+\mathrm{Pr}^{-1})^{-1/2}(1-0.5s+2sy)^{-1/2}(1-0.5s+sy)y^{1/2}$. A linear fit is seen in this figure suggesting the proposed scale relation in Eq. (32) can reasonably describe the motion of the steady-state boundary layer at different streamwise locations and at various working conditions and R^2 of the fitted line is 0.96063.

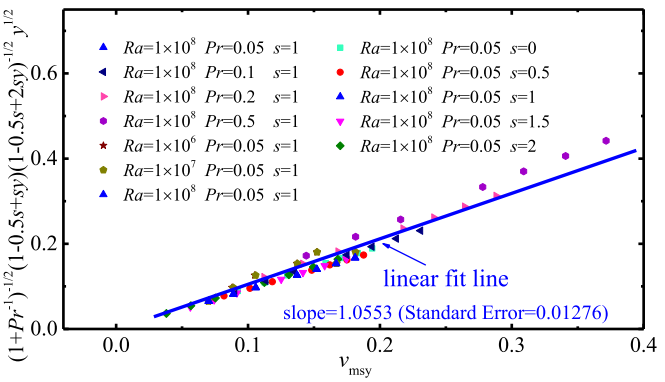

FIG. 16. Scale of $(1+\mathrm{Pr}^{-1})^{-1/2}(1-0.5s+2sy)^{-1/2}(1-0.5s+sy)y^{1/2}$ vs numerically obtained v_{msy} at the steady state.

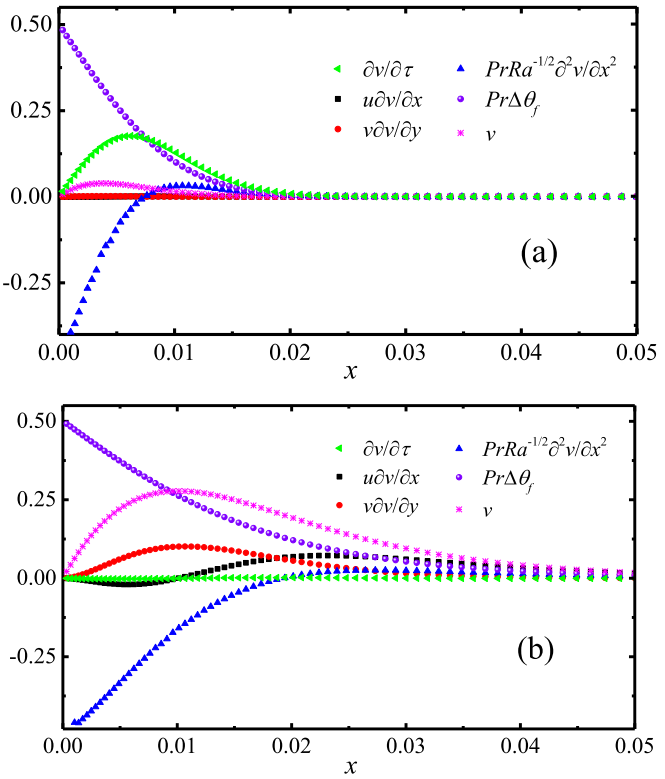

FIG. 17. Horizontal profiles of the unsteady term, horizontal advection term, vertical advection term, buoyancy term, viscous term, and velocity with the case $\mathrm{Ra}=1\times10^8$, $\mathrm{Pr}=0.5$, $s=1$ at a streamwise location of $y=0.5$. (a) Start-up state (at $\tau=0.22\,\tau_{sy}$); (b) Steady state (at $\tau=6.57\tau_{sy}$).

The horizontal profiles of the various terms describing the unsteady vertical momentum of the present $\mathrm{Pr}<1$ fluids are plotted in Fig. 17(a), and the corresponding data are obtained at a time instance of $\tau=0.22\,\tau_{sy}$. It is seen in this figure that the buoyancy, the vertical advection, and the viscous terms are of equivalent significance, and all other terms are much smaller at the initial growth state which confirms the corresponding analysis in Sec. III. Figure 17(b) further presents the profiles at the steady state, at $\tau=6.57\tau_{sy}$. It is seen that the unsteady term decreases to approximately zero at this state, leaving the buoyancy and viscous terms still the most important ones and confirming the force balances utilized for deriving the scales in Sec. III.

V. CONCLUSION

The convective boundary layer flow induced by linearly heating an initially isothermal and quiescent fluid is investigated by a scaling analysis in this study.

The derived scaling relations demonstrate that the flow mechanism of the $\mathrm{Pr}<1$ and $\mathrm{Pr}>1$ fluids are fundamentally different, and the two flows are described by different sets of scaling laws. It is also found that the convective boundary layer flow first experiences an initial growth state, and it eventually transits to a fully steady state after the LEE is fully

convected away. The scaling analysis further reveals that unlike the extensively studied homogenously heating problem, which is featured by a one-dimensional initial growth state and a two-dimensional fully developed state, the present flow problem is consistently two-dimensional as long as $s \neq 0$, i.e., a nonzero background temperature stratification. The derived scaling relations are compared with the DNS results, and a good agreement is achieved.

It is also primarily found from the current DNS calculations that the oscillatory amplitude of the flow parameters associated with the LEE reduces with increasing the temperature stratification factor, s, at $\mathrm{Pr} > 1$. This may merit a separate study in the future.

ACKNOWLEDGMENTS

The DNS calculations were physically performed by Mr. Sitao Ren, and the corresponding work is gratefully acknowledged. The financial support from the Fundamental Research Funds for the Central Universities of China (DUT19LK23) is also gratefully acknowledged. Comments from the anonymous reviewers are also gratefully acknowledged.

[1] L. Prandtl, On fluid motions with very small friction, in *Proceedings of the 3rd International Mathematical Congress, Heidelberg, Germany, 8–13 August* (B.G. Teubner, Leipzig, Germany, 1904), pp. 484–491.

[2] L. Prandtl, *Essentials of Fluid Dynamics: With Applications to Hydraulics, Aeronautics, Meteorology and Other Subjets* (Blackie and Son, London, 1953).

[3] F. Xu, J. C. Patterson, and C. Lei, Transition to a periodic flow induced by a thin fin on the sidewall of a differentially heated cavity, Int. J. Heat Mass Transfer **52**, 620 (2009).

[4] S. C. Saha, Unsteady natural convection in a triangular enclosure under isothermal heating, Energy Build. **43**, 695 (2011).

[5] Y. Zhao, C. Lei, and J. C. Patterson, Resonance of the thermal boundary layer adjacent to an isothermally heated vertical surface, J. Fluid Mech. **724**, 305 (2013).

[6] Y. Liu, C. Lei, and J. C. Patterson, Natural convection in a differentially heated cavity with two horizontal adiabatic fins on the sidewalls, Int. J. Heat Mass Transfer **72**, 23 (2014).

[7] Y. Liu, C. Lei, and J. C. Patterson, Plume separation from an adiabatic horizontal thin fin placed at different heights on the sidewall of a differentially heated cavity, Int. Commun. Heat Mass Transfer **61**, 162 (2015).

[8] A. Scagliarini, Á. Gylfason, and F. Toschi, Heat-flux scaling in turbulent Rayleigh-Bénard convection with an imposed longitudinal wind, Phys. Rev. E **89**, 043012 (2014).

[9] J. Ma and F. Xu, Unsteady natural convection and heat transfer in a differentially heated cavity with a fin for high Rayleigh numbers, Appl. Therm. Eng. **99**, 625 (2016).

[10] Y. Liu, S. Zhang, H. Huang, Q. Suo, Y. Bian, and Y. Zhao, Enhancing the flow and heat transfer in a convective cavity using symmetrical and adiabatic twin fins, Int. J. Heat Mass Transfer **142**, 118447 (2019).

[11] W. Lin and S. W. Armfield, Natural convection boundary-layer flow on an evenly heated vertical plate with time-varying heating flux in a stratified $\mathrm{Pr} < 1$ fluid, Num. Heat Transfer A **76**, 393 (2019).

[12] Y. Zhao, P. Zhao, Y. Liu, Y. Xu, and J. F. Torres, On the selection of perturbations for thermal boundary layer control, Phys. Fluids **31**, 104102 (2019).

[13] S. W. Armfield and R. Janssen, A direct boundary-layer stability analysis of steady-state cavity convection flow, Int. J. Heat Fluid Flow **17**, 539 (1996).

[14] J. Tao, Nonlinear global instability in buoyancy-driven boundary-layer flows, J. Fluid Mech. **566**, 377 (2006).

[15] Z. Gao, B. Podvin, A. Sergent, S. Xin, and J. Chergui, Three-dimensional instabilities of natural convection between two differentially heated vertical plates: Linear and nonlinear complementary approaches, Phys. Rev. E **97**, 053107 (2018).

[16] N. A. Pelekasis, Linear stability analysis and dynamic simulations of free convection in a differentially heated cavity in the presence of a horizontal magnetic field and a uniform heat source, Phys. Fluids **18**, 034101 (2006).

[17] A. Aziz, A similarity solution for laminar thermal boundary layer over a flat plate with a convective surface boundary condition, Commun. Nonlinear Sci. Numer. Simul. **14**, 1064 (2009).

[18] A. Ishak, Similarity solutions for flow and heat transfer over a permeable surface with convective boundary condition, Appl. Math. Comput. **217**, 837 (2010).

[19] T. Chen, E. Sparrow, and A. Mucoglu, Mixed convection in boundary layer flow on a horizontal plate, J. Heat Transfer **99**, 66 (1977).

[20] J. C. Patterson and J. Imberger, Unsteady natural convection in a rectangular cavity, J. Fluid Mech. **100**, 65 (1980).

[21] W. Lin and S. Armfield, Long-term behavior of cooling fluid in a rectangular container, Phys. Rev. E **69**, 056315 (2004).

[22] W. Lin, S. W. Armfield, and J. C. Patterson, Cooling of a $\mathrm{Pr} < 1$ fluid in a rectangular container, J. Fluid Mech. **574**, 85 (2007).

[23] W. Lin, S. W. Armfield, J. C. Patterson, and C. Lei, Prandtl number scaling of unsteady natural convection boundary layers for $\mathrm{Pr} > 1$ fluids under isothermal heating, Phys. Rev. E **79**, 066313 (2009).

[24] W. Lin and S. Armfield, Unified Prandtl number scaling for start-up and fully developed natural-convection boundary layers for both $\mathrm{Pr} \gtrsim 1$ and $\mathrm{Pr} \lesssim 1$ fluids with isothermal heating, Phys. Rev. E **86**, 066312 (2012).

[25] W. Lin and S. W. Armfield, Unsteady natural convection on an evenly heated vertical plate for Prandtl number $\mathrm{Pr} < 1$, Phys. Rev. E **72**, 066309 (2005).

[26] W. Lin and S. Armfield, Scalings for unsteady natural convection boundary layers on an evenly heated plate with time-dependent heating flux, Phys. Rev. E **88**, 063013 (2013).

[27] W. Lin, S. W. Armfield, and P. L. Morgan, Unsteady natural convection boundary-layer flow along a vertical isothermal plate in a linearly stratified fluid with $\mathrm{Pr} > 1$, Int. J. Heat Mass Transfer **45**, 451 (2002).

[28] Y. Liu, Y. Bian, Y. Zhao, S. Zhang, and Q. Suo, Scaling laws for the transient convective flow in a differentially and linearly

heated rectangular cavity at Pr > 1, Phys. Fluids **31**, 043601 (2019).

[29] F. Xu, J. C. Patterson, and C. Lei, Transient natural convection flows around a thin fin on the sidewall of a differentially heated cavity, J. Fluid Mech. **639**, 261 (2009).

[30] B. Nie and F. Xu, Scales of natural convection on a convectively heated vertical wall, Phys. Fluids **31**, 024107 (2019).

[31] S. V. Patankar and D. B. Spalding, A calculation procedure for heat, mass and momentum transfer in three-dimensional parabolic flows, Int. J. Heat Mass Transfer **15**, 1787 (1972).

[32] B. P. Leonard, A stable and accurate convective modelling procedure based on quadratic upstream interpolation, Comput. Meth. Appl. Mech. Eng. **19**, 59 (1979).